Synergetic Effect of MoS_2 and Graphene on Ag_3PO_4 for its Ultra-Enhanced Photocatalytic Activity in Phenols Degradation under Visible Light

Wen-chao Peng [1], Xi Wang [1,2] and Xiao-yan Li[1]*

[1] Environmental Engineering Research Centre, Department of Civil Engineering, The University of Hong Kong, Pokfulam Road, Hong Kong

[2] School of Chemistry and Environment, South China Normal University, Guangzhou, Guangdong, China

(*Corresponding author: phone: 852 2859-2659; fax: 852 2859-5337; e-mail: xlia@hkucc.hku.hk)

Abstract

The photo-degradation of organic pollutants using solar light is an attractive chemical process for water pollution control. In this study, we synthesized a new composite material consisting of silver phosphate (Ag_3PO_4) sub-microcrystals grown on a layered molybdenum disulfide (MoS_2) and graphene (GR) hybrid as a high-performance photocatalyst for the degradation of toxic organic pollutants. This composite photocatalyst was prepared via a simple two-step hydrothermal process that used sodium molybdate, thiourea and graphene oxide as precursors for the MoS_2/GR hybrid and silver nitrate for the Ag_3PO_4 sub-microcrystals. The composite Ag_3PO_4-0.02(MoS_2/0.005GR) was found to be the most effective catalyst for the photo-decomposition of 2,4-dichlorophenol under simulated solar light and visible light ($\lambda \geq 420$ nm). The photocatalyst was also highly active for the degradation of nitrophenol and chlorophenol. The ultra photocatalytic activity of the novel

25 catalyst arose from the synergetic effects of MoS_2 and GR as cocatalysts in the composite.
26 MoS_2/GR nanosheets served as electron collectors for the interfacial electron transfer from
27 Ag_3PO_4 to electron acceptors in the aqueous solution and thus enhanced the separation of the
28 photo-generated electron-hole pairs and made the holes more available for organic oxidation.
29 In addition, the presence of MoS_2 and GR provided more active adsorption sites and allowed
30 for the activation of dissolved O_2 for organic degradation in water.

31 **Keywords:** Silver phosphate (Ag_3PO_4); Molybdenum disulfide (MoS_2); graphene; phenol
32 degradation; photocatalysis; visible light

33

34 **1. Introduction**

35 Photocatalysis is an attractive technology for treating pollutants in water using solar
36 energy.[1] Since the discovery of photocatalytic water splitting by titania,[2] significant efforts
37 have been devoted to the development of more active photocatalysts for environmental
38 applications.[3, 4] Of particular interest is synthesizing catalysts that are highly active under
39 visible light.[5] Silver orthophosphate (Ag_3PO_4) was recently shown to be an effective
40 photocatalyst for O_2 evaluation and dye degradation under solar light.[6, 7] It was reported that
41 Ag_3PO_4 can achieve a quantum efficiency of about 90% at a wavelength of around 420 nm,
42 which is significantly higher than most of the other semiconductors previously reported.[6, 7]
43 Moreover, with effective control of the morphology, the facet photocatalytic effect can be
44 achieved for Ag_3PO_4.[7] However, the photocatalytic efficiency of bare Ag_3PO_4 remains low
45 due to its low response to visible light and the high recombination rate of photo-generated
46 electron-hole pairs.[8] Ag_3PO_4-based materials therefore require modifications to achieve a
47 much higher photocatalytic activity for use in detoxification and degradation of contaminants
48 in water.[8-11]

Graphene (GR), a versatile carbon material with a single layer and sp^2-hybridized carbon lattice, possesses excellent electrical, thermal and mechanical properties.[12] As GR can serve as an excellent charge carrier at room temperature (200,000 $cm^2V^{-1}s^{-1}$), it has attracted increasing attention in the photocatalysis field.[4, 13] Using GR to form electron-conducting surfaces and channels, the photocatalytic activity of composite materials can be greatly increased, mainly owing to the effective separation of the electron-hole pairs.[14, 15] Molybdenum disulfide (MoS_2) is another emerging photocatalytic cocatalyst material that may be used as a substitute for noble metals in photocatalyst synthesis. It has been reported that MoS_2 has a layered structure consisting of Mo-S-Mo sandwiched in a graphite-like manner by the relatively weak van der Waals force.[16] The edge site activity of MoS_2 is comparable to Pt nanoparticles as a cocatalyst for the photocatalytic hydrogen generation.[17] Moreover, nanoscale MoS_2 is a reportedly good O_2-activation cocatalyst for oxidation reactions.[20] This feature facilitates the formation of superoxide radical anions (O_2^-) during the photo-oxidation process.[4] Various MoS_2-based nanomaterials such as nanosheets and nanoparticles have shown a great potential as cocatalysts for photocatalysis.[19, 21] A number of composite material systems such as MoS_2-TiO_2,[22] MoS_2-CdS[21, 23] and MoS_2-kaolin[24] have received attention for their high performance in photocatalytic pollutant degradation.

In this study, we synthesized the Ag_3PO_4 sub-microcrystals supported on a layered MoS_2/graphene hybrid to form a composite photocatalyst for the degradation of organic phenols under simulated solar light or visible light. Phenolic chemicals, especially those with nitro and chloric groups, are highly toxic and recalcitrant to biological treatment processes and harmful to the environment.[25, 26] Photocatalysis can be an effective strategy for destructing and degrading organic phenols in water.[27-29] The contents of MoS_2 and GR and their hybrid incorporations are optimized in the novel Ag_3PO_4-MoS_2/GR composite photocatalyst. This composite was shown to be a visible light-response catalyst that exhibited

a great photocatalytic activity for the degradation of model organic phenols, including phenol and phenols with chloro- and nitro- substituents.

2. Experimental Materials and Methods

2.1 Synthesis of MoS_2/GR nanosheets

The GO was synthesized from natural graphite powder using a modified Hummers method.[30] In a typical synthesis of the MoS_2/GR hybrid, 0.242 g (1 mmol) of $Na_2MoO_4 \cdot 2H_2O$ and 0.38 g (5 mmol) of thiourea were dissolved in 60 mL of deionized (DI) water, into which 13.5 mg of the prepared GO were added. The homogeneous solution was then placed in a 100-mL Teflon-lined autoclave and held at 210°C for 24 h. The black precipitates formed in the solution were then collected by centrifugation, washed three times with DI water and ethanol and then dried in an oven at 80°C for 12 h.[31]

2.2 Synthesis of the Ag_3PO_4-MoS_2/graphene composite

A pre-predetermined amount of the MoS_2/GR composite was dispersed in 40 mL DI water via sonication. 1.02 g $AgNO_3$ (6 mmol) was then stirred into the solution, followed by dropwise dosing of 10 mL of a 0.2 M Na_2HPO_4 solution (2 mmol). The mixture was stirred for 4 h while precipitates were formed. The precipitates were separated by filtration and then washed with ethanol and DI water five times. The product was then dried at 60°C for 24 h.[8] The Ag_3PO_4 crystals were prepared following the same method without the addition of MoS_2 or the MoS_2/GR hybrid.

2.3 Photocatalytic degradation of phenols

The photocatalytic decompositions of DCP and other phenolic compounds were performed in a photo-reactor. During a typical test on DCP degradation, 20 mg of the

photocatalyst was dispersed in 50 mL of water in a quartz photo-tube via sonication, and DCP was then added to an initial concentration of 20 mg/L. Before being exposed to light, the suspension was stirred in the dark for 4 h to allow the catalysts to adsorb DCP in the solution. After adsorption, the DCP was photocatalyzed in an XPA-7 photo-reactor (Xujiang Electromechanical Plant, Nanjing, China) with a 500-W xenon lamp serving as the simulated solar (SS) light source. In addition, for the photo-tests under visible light, a light filter (>420 nm) was inserted to eliminate UV light from the light source. During the photocatalytic process, 1 mL of the solution was sampled from the photo-tube at regular intervals to monitor the change in DCP concentration. The samples were filtered by a syringe filter (0.2 μm), and the DCP concentrations were measured by high-performance liquid chromatography (HPLC, Waters 2695, with a photodiode array detector). The analysis of other phenols was also performed using the HPLC with the same mobile phase (acetonitrile:H_2O=40:60) and different detection wavelengths (phenol: 270 nm, DCP: 287 nm, 2-CP: 276 nm and 4-NP: 316 nm).

2.4 Material characterizations

An X-ray diffraction (XRD) system (Bruker D8 Advance X-ray Powder Diffractometer) was used to analyze the crystal forms of the photocatalytic materials. Scanning electron microscopy (SEM, Hitachi S-4800) was used to examine the morphology of the catalysts and to analyze the elemental composition of the catalysts from the energy-dispersive X-ray spectroscopy (EDX). Transmission electron microscopy (TEM, Philips Tecnai G220 S-TWIN) was used to analyze the structure details of the catalyst materials from the TEM and high-resolution TEM (HRTEM) images. Raman spectra of the samples were recorded with an inVia Raman microscope (Renishaw). Fourier transform infrared (FT-IR) spectroscopy (Spectrum One B, Perkin Elmer) was used to characterize the functional groups of the composite catalysts. The UV-vis diffusive reflectance spectra of the powder photocatalysts

were analyzed by a spectrophotometer (Hitachi U-3010). The photoluminescence (PL) spectra of the photocatalysts were measured by Hitachi F-7000 Fluorescence Spectrophotometer with an excitation wavelength of 440 nm. The photoelectric conversion property of the photocatalyst materials was tested using a three-electrode cell connected to a computer-controlled potentiostat (Princeton VersaSTAT 4) (the test details are given in Electronic Supplementary Information (ESI†)). A Beckman Coulter SA3100 surface area analyzer was used to determine the surface area and pore structure of the catalyst powder samples from the nitrogen adsorption-desorption isotherm at liquid nitrogen temperature (77 K).

3. Results and Discussion

3.1 Characterization of the photocatalysts

The Ag_3PO_4-MoS_2/GR composite photocatalysts were synthesized by a facial two-step hydrothermal method as illustrated in Fig. 1. The layered MoS_2/GR was first synthesized by the hydrothermal reaction of Na_2MoO_4 and H_2CSNH_2 in an aqueous solution of graphene oxide (GO) at 210°C for 24 h.[31] During the process, GO was reduced to GR, on which GR-like MoS_2 nanosheets were formed (see Fig. S1 in ESI†). The MoS_2/GR hybrid and $AgNO_3$ precursors were subsequently dispersed in DI water with sonication. Na_2HPO_4 was then added to precipitate Ag_3PO_4 sub-micro particles on the MoS_2/GR surface, producing the final Ag_3PO_4-MoS_2/GR composite.[8]

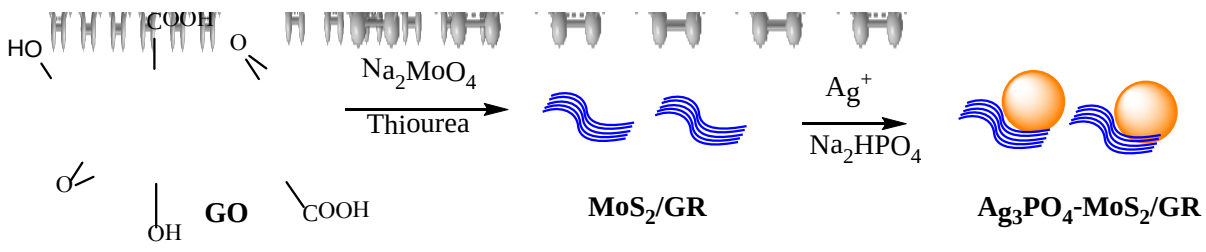

Fig. 1. Illustration of the Ag_3PO_4-MoS_2/GR photocatalyst synthesis.

Figs. 2a and 2b show the SEM and TEM images of the as-prepared MoS_2/GR hybrid. A flower-like morphology can be seen for the hybrid, and the GR sheets mesh uniformly with the MoS_2 nanosheets. More detailed crystal lattice is presented in Fig. S1b (ESI†). As shown in Fig. 2c, pure Ag_3PO_4 precipitates were formed as spherical particles. For the composite in Fig. 2d, most of the Ag_3PO_4 were sub-micro particles that were covered by irregular sheets of the MoS_2/GR hybrid (SEM photos are shown in Fig. S2, ESI†). The EDX spectra and elemental mapping images in Fig. S3 (ESI†) directly show the content and distribution of the elements for the Ag_3PO_4-MoS_2/GR composite. The FT-IR profiles in Fig. S4a (ESI†) indicate the reduction from GO to GR during the preparation of the MoS_2/GR hybrid. Most of the functional groups of GO, including 1,630 cm^{-1} for COO, 1,392 cm^{-1} for O-H and 1,085 cm^{-1} for C-O, disappeared after the chemical reduction. Compared with pure Ag_3PO_4, however, no obvious new FT-IR peaks were identified for the Ag_3PO_4-MoS_2/GR composite due to the low percentage of MoS_2/GR hybrid in the composite (Fig. S4b, ESI†).

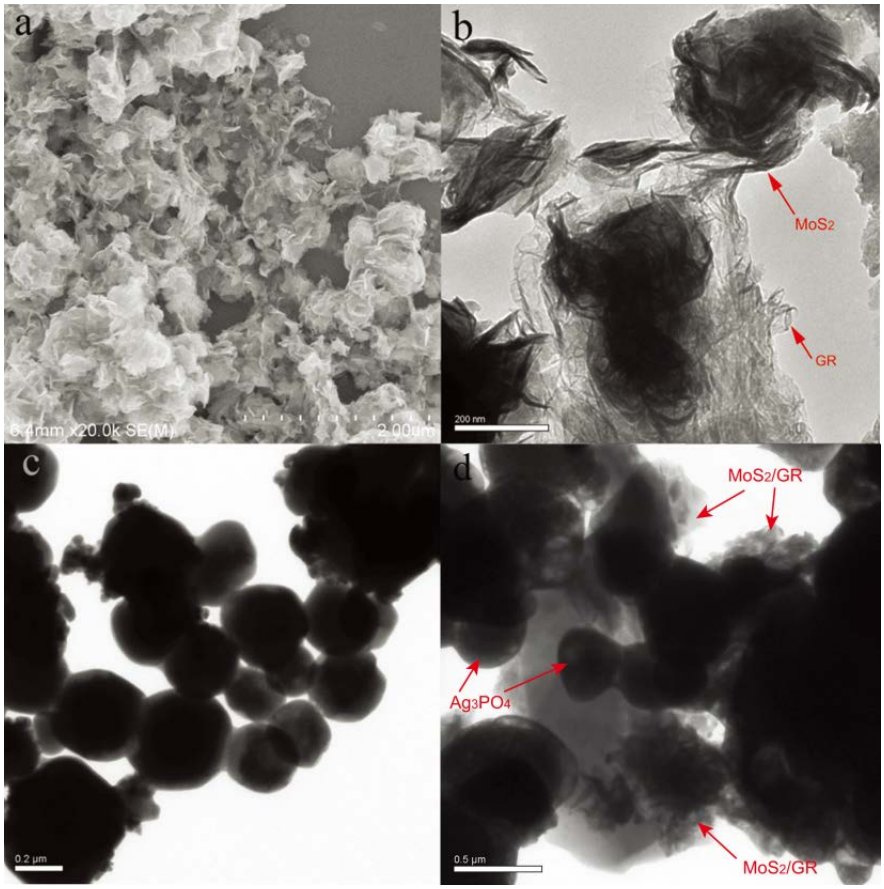

158

159 Fig. 2. (a) SEM and (b) TEM photos of the MoS_2/GR hybrid. TEM photos of (c) pure

160 Ag_3PO_4 and (d) the Ag_3PO_4-MoS_2/GR composite.

161 The Raman spectra of the catalyst materials are given in Fig. 3. Several of the peaks

162 below 1,200 cm^{-1} corresponded with the Ag_3PO_4 vibrations. Two peaks at 1,330 cm^{-1} (D

163 peak) and 1,590 cm^{-1} (G peak) were also observed, confirming the presence of GR in the

164 Ag_3PO_4-MoS_2/GR composite.[8] Compared with the GO (I_D/I_G=1.10), a lower I_D/I_G intensity

165 ratio (I_D/I_G=0.90) was found in the GR, suggesting an increase in the proportion of sp^2

166 conjugated carbon atoms.[32] It is apparent that the sp^3 hybridized carbon atoms were restored

167 to sp^2 conjugation during the hydrothermal treatment process. In addition, the G band

168 downshifted from 1,589.1 to 1,587.1 cm^{-1}.[33] The decrease in I_D/I_G and the downshift of the G

169 band indicated a successful reduction from GO to GR after the hydrothermal treatment.

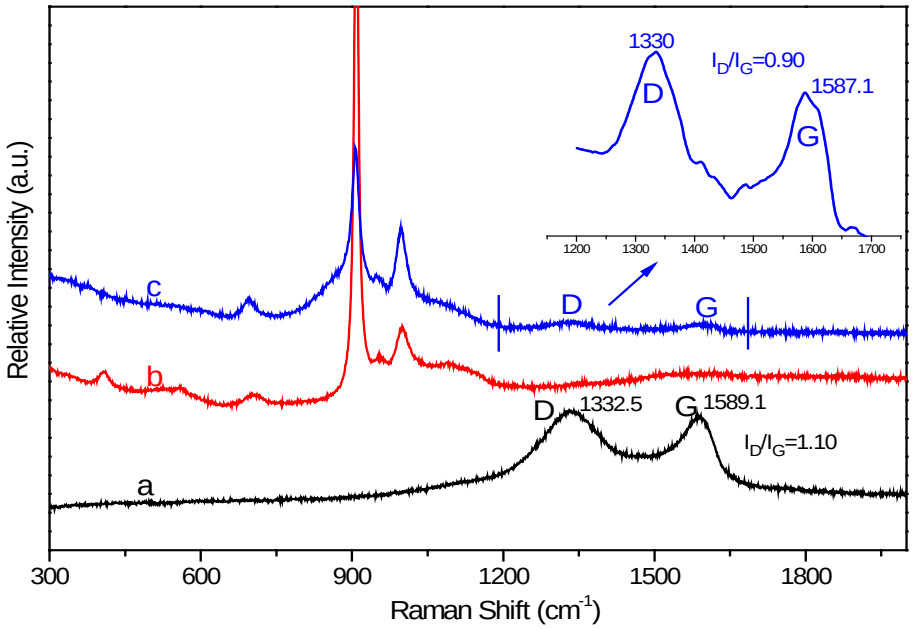

Fig. 3. Raman spectra of (a) GO, (b) pure Ag_3PO_4 and (c) the Ag_3PO_4-MoS_2/GR composite. The inset figure shows a selected portion of spectrum (c).

Fig. 4 shows the XRD spectra of the MoS_2/GR hybrid and Ag_3PO_4-MoS_2/GR composite. The high-temperature hydrothermal treatment was beneficial to the formation of MoS_2 nanosheets with a good crystal form (inset of Fig. 4). All of the characteristic peaks of Ag_3PO_4 could be found for pure Ag_3PO_4 and the composites, and no obvious difference was identified between them due to the small percentage and weak intensity of MoS_2 and GR in the composite. The N_2-adsorption results for pure Ag_3PO_4 and the composites are shown in Fig. S5 (ESI†). Compared with the Ag_3PO_4 crystals, GR had a larger surface area and a higher adsorption capacity. However, little improvement in adsorption capability was made for the Ag_3PO_4-MoS_2/GR composite, probably due to the low percentage of GR dosed. The GR content was also too low to change the pore structures of the composites (Fig. S5).

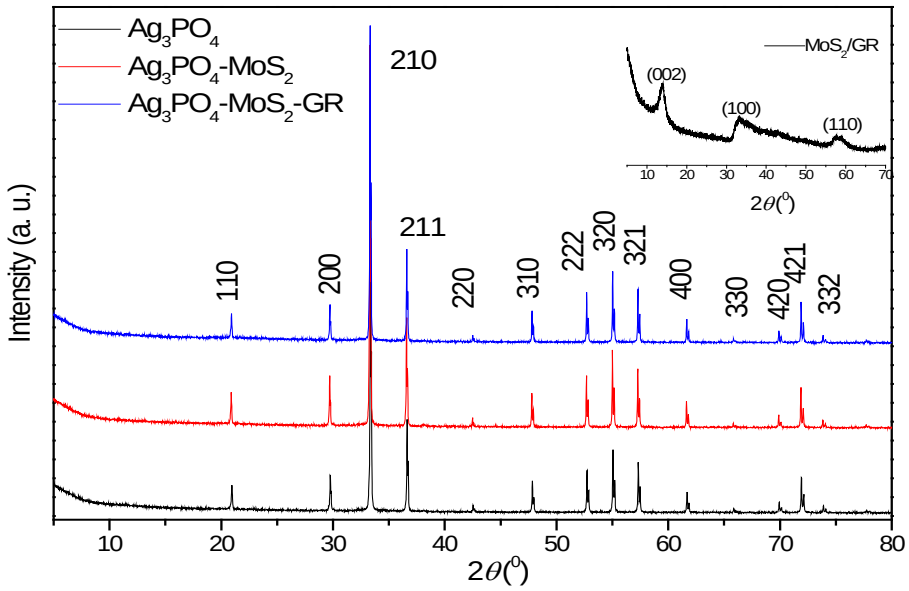

Fig. 4. XRD patterns of the pure Ag_3PO_4 and its composite materials. The inset of the figure shows the XRD pattern of the MoS_2/GR hybrid.

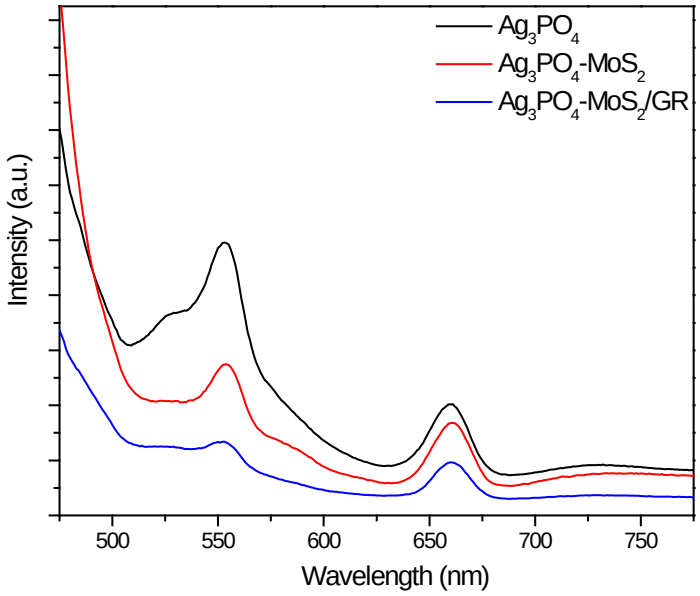

Fig. 5. Photoluminescence spectra of Ag_3PO_4, Ag_3PO_4-MoS_2 and Ag_3PO_4-MoS_2/GR for an excitation wavelength of 440 nm.

A photoluminescence (PL) spectrum can be used for a material to show the dynamics of the separation and recombination of photo-induced electrons and holes.[34, 35] As presented in

Fig. 5, pure Ag_3PO_4 sub-microcrystals exhibit a strong and wide PL peak at around 555 nm and a small PL peak at around 660 nm, which display the re-radiation of photons from the recombinations of electron-hole pairs. With the dosing of MoS_2 nanosheets into Ag_3PO_4, the intensity of both PL peaks decreased clearly, and incorporation of the MoS_2/GR hybrid could further decrease the peak intensity. The comparison of PL spectra between the three materials indicates a reduced intensity of photon radiation from the electron-hole recombinations when MoS_2 or MoS_2/GR nanosheets were incorporated with Ag_3PO_4. It is evidenced that photo-induced electrons on Ag_3PO_4 could migrate through the conducting nanosheets, reducing the subsequent electron-hole combinations.[35, 36] Therefore, the use of MoS_2 and GR can improve the charge separation efficiency and enhance the photocatalytic activity of Ag_3PO_4.

Furthermore, photocurrent is also an effective measurement of the photo-activity of a semiconductor. The photocurrents yielded from the electrodes of pure Ag_3PO_4, Ag_3PO_4-MoS_2 and Ag_3PO_4-MoS_2/GR on a tin-doped indium oxide (ITO) glass were measured in a 0.01 M Na_2SO_4 aqueous solution under visible light ($\lambda \geq 420$ nm). As shown in Fig. S6 (ESI†), the Ag_3PO_4-MoS_2/GR composite displayed the highest photo-electric conversion, with a photocurrent value of as high as 2.5 mA. Pure Ag_3PO_4 had the lowest performance in photo-electric conversion with a photocurrent of only 0.2 mA. The photocurrent comparison is consistent with that of the PL spectra for the photocatalyst materials (Ag_3PO_4, Ag_3PO_4-MoS_2 and Ag_3PO_4-MoS_2/GR). The results further proved that incorporation of the MoS_2/GR hybrid can greatly enhance the photocatalytic activity of the Ag_3PO_4-based composite catalyst.

3.2 Photocatalytic activity for the decomposition of phenols

The photocatalytic activity of different catalyst materials was then tested for the degradation of phenols under solar light. DCP was initially selected as the model substrate, and a 500-W Xeon light source without a light filter was used to simulate the solar light

condition. As shown in Fig. 6a, while the weight percentage of the MoS_2/GR hybrid in the composites was fixed at 2%, the GR content in the hybrid varied. The pure Ag_3PO_4 showed a low photocatalytic activity (75% DCP degradation in 60 min). The addition of the layered MoS_2/GR cocatalyst improved the photo-activity of the Ag_3PO_4 significantly. The best DCP degradation result was obtained with the MoS_2/0.005GR hybrid incorporated in the photocatalyst. A further increase of the GR content in the cocatalyst led to a gradual reduction of the photo-activity of the catalyst. Thus, the MoS_2/0.005GR hybrid was determined to compose the cocatalyst.

The content of the cocatalyst (MoS_2/0.005GR) was also optimized for the synthesis of the photocatalyst based on the DCP degradation result (Fig. 6b). As indicated by the diffusive reflectance spectra (Fig. S7, ESI†), addition of the cocatalyst (MoS_2/GR) can increase the ability of the catalyst to absorb visible light. Moreover, as discussed previously, the layered MoS_2/GR conduct sheets can enhance the transfer of electrons from Ag_3PO_4 to the receiving medium in the solution. Both effects would lead to an increase in the photocatalytic activity of the composite catalyst for organic oxidation. However, a further increase in the amount of cocatalyst (MoS_2 and GR) would result in a shielding effect of the dosing materials on the main photocatalyst. A higher percent of dark cocatalyst not only shields the active sites on the catalyst surface but also decreases the depth of light penetration into the solution and the photocatalyst. Such a “shielding effect” or “masking effect” would hinder the photocatalytic activity of the catalyst. [15, 37, 38] Therefore, the amount of the cocatalyst should be optimized, and composite Ag_3PO_4-0.02(MoS_2/0.005GR) was found to possess the best photocatalytic property for the DCP degradation.

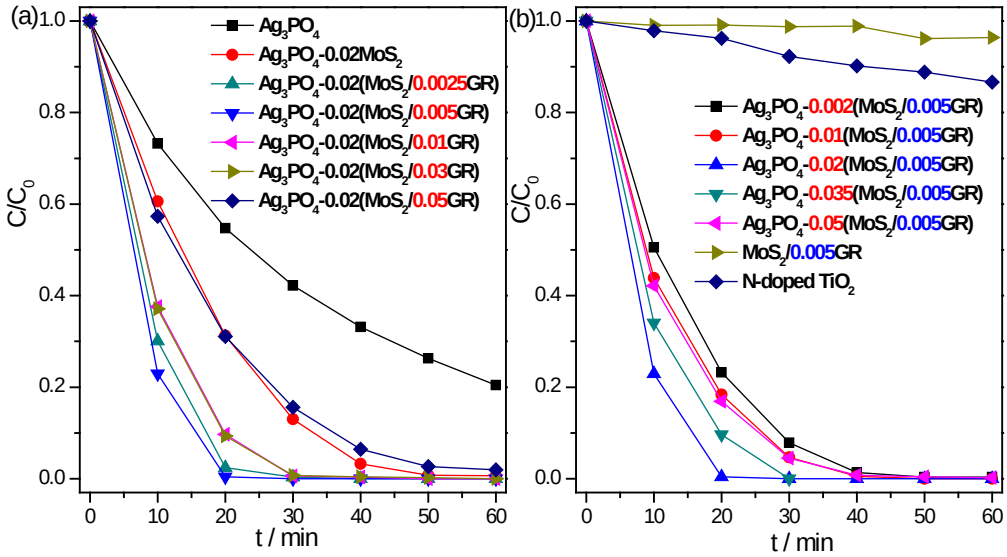

Fig. 6. Photocatalytic DCP degradation by the photocatalysts under SS light (a) with the different GR contents and (b) with the different MoS_2/0.005GR percentages.

Additionally, the photocatalytic activity of only MoS_2/0.005GR without Ag_3PO_4 was also tested, and the results showed no DCP degradation under visible light (Fig. 6b). It is apparent that the MoS_2/GR hybrid alone is not an effective photocatalyst; however, the hybrid can function as an effective cocatalyst to enhance the photocatalytic activity of Ag_3PO_4. With the optimized composition (2% cocatalyst), DCP degradation (20 ppm) was nearly completed in 20 min under simulated solar light. To evaluate the photo-activity of the new composite catalysts, nitrogen-doped TiO_2 was used as a comparison in the photo-degradation test. However, this commonly used photocatalyst only degraded ~4% of the DCP in 20 min under the same conditions. The photo-activity of the catalysts under visible light (λ>420 nm) were also tested for DCP decomposition. As shown in Fig. 7, the composite photocatalysts appeared to be highly active to degrade DCP under visible light. The results proved that the Ag_3PO_4-MoS_2/GR composite is a visible light-responsive photocatalyst. As expected, the rates of DCP degradation under visible light were somewhat slower than the rates recorded in Fig. 6 under solar light.

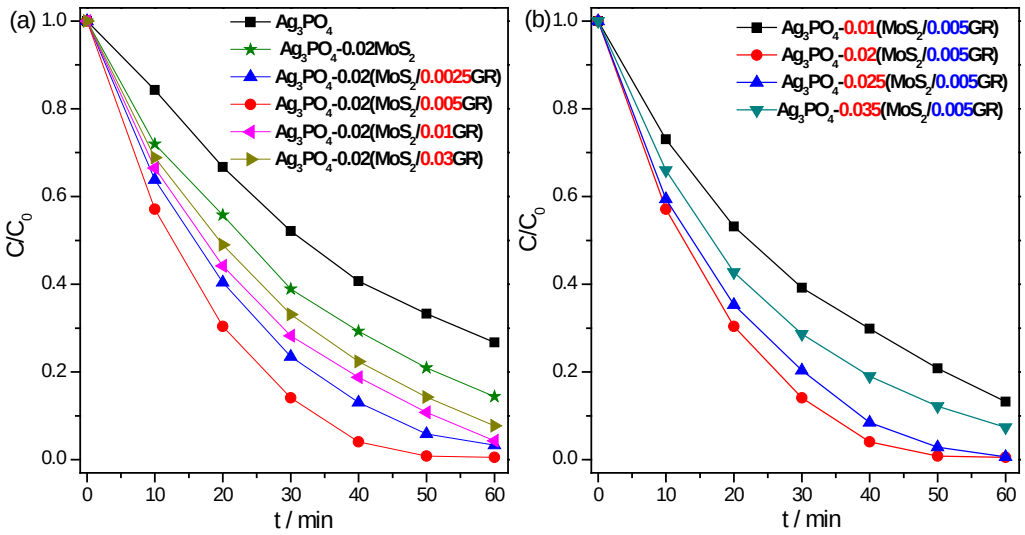

Fig. 7. Photocatalytic DCP degradation by the photocatalysts under visible light (λ>420 nm) (a) with the different GR contents and (b) with the different MoS_2/0.005GR percentages.

The photocatalytic decomposition of DCP by the Ag_3PO_4-MoS_2/GR composite was further verified. The adsorption capability of the composite photocatalyst was tested for DCP without light, and the results are presented in Fig. S8 (ESI†). For the small amount (≤2%) of MoS_2 and GR incorporated in the catalyst, its contribution to the chemical removal by adsorption is expected to be limited. In fact, ≤5% of the model organic, i.e., DCP, was removed by adsorption from the solution. Hence, photocatalysis is shown to be the predominant mechanism for the DCP degradation observed. According to the FTIR spectra of the DCP samples (Fig. S9A, ESI†), the peak for the phenolic hydroxyl group shifted from 3226 to 3100 cm^{-1}, indicating the dechlorination result after the photocatalysis.[39] Moreover, the HPLC profiles of the DCP solution further confirmed the change of chemicals after the photo-degradation test (Fig. S9B, ESI†). All of these experimental results proved that the observed DCP removal was brought about by photocatalytic decomposition other than adsorption. Besides the photo-reactivity, the stability of the composite Ag_3PO_4-MoS_2/GR photocatalyst was also tested. According to the performance of the photocatalyst for DCP

degradation (Fig. S10, ESI†), no significant deactivation was found for the recycled catalyst after three test runs.

To further verify the activity of the optimized catalyst Ag_3PO_4-0.02(MoS_2/0.005GR), more organic phenols with different functional groups were selected as substrates for the photocatalytic degradation. The results in Fig. 8a show that the new photocatalyst was highly effective in the degradation of every selected phenolic compound. More than 50% of the 4-nitrophenol in the solution, which is one of the most recalcitrant organic phenols, was degraded in 60 min under the SS light. When visible light was used, no great photo-activity decrease was observed, indicating the good visible light response of the composite photocatalyst (Fig. 8b).

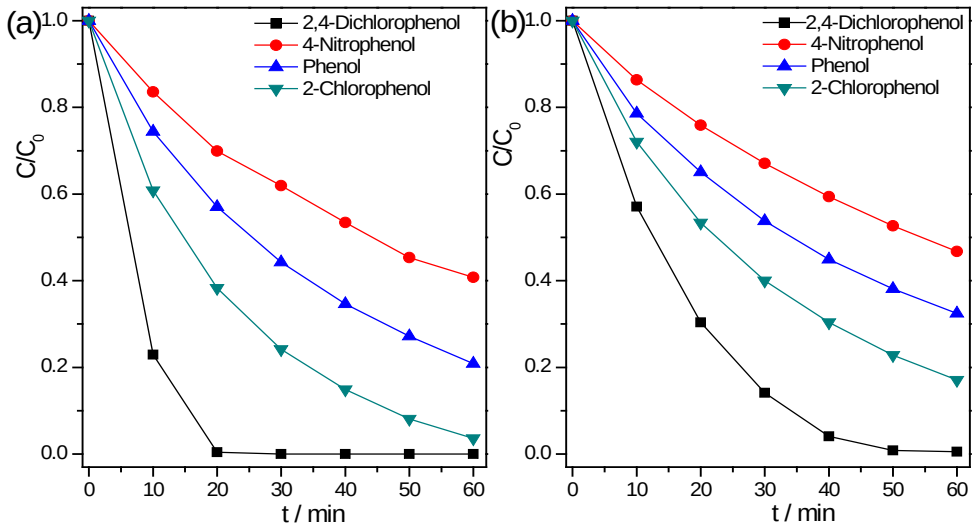

Fig. 8. Degradation of different organic phenols under (a) SS light and (b) visible light ($\lambda \geq 420$ nm).

The specific schematics for the photocatalytic degradation of DCP by the Ag_3PO_4-MoS_2/GR composite are illustrated in Fig. S11 (ESI†). The DCP molecules were readily adsorbed by the benzene structure of the GR via conjugation, which was beneficial to the subsequent DCP degradation reactions. The Ag_3PO_4 acted as a semiconductor with a CB of

0.45 eV and a VB of 2.45 eV. Under the solar light, electrons were excited from VB to CB, inducing the formation of holes at the VB. The large surface area and excellent conductivity of GR sheets allow the transfer of photo-excited electrons from Ag_3PO_4 to the terminal electron accepting medium, i.e., dissolved oxygen (DO), in water.[40] Hence, the use of MoS_2/GR nanosheets can greatly improve the interfacial charge transfer between the photocatalyst and the aqueous solution. As presented by the energy diagram and electron transfer scheme in Fig. S11 (ESI†), the improved electron transfer to DO molecules would enhance the separation of the electron-hole pairs, making the holes more available for organic oxidation. [8, 20]

Meanwhile, the MoS_2/GR nanosheets would also function as effective electron collectors to facilitate the charge transfer between the photo-generated holes on the catalyst and organic molecules (electron donors) in the solution, which improved the efficiency of photocatalytic organic oxidation. The holes could directly oxidize the DCP molecules adsorbed on the catalyst surface. Moreover, the holes reacted with water (or hydroxyl) to form hydroxyl free radicals (·OH),[4, 41] which are a strong oxidant for DCP decomposition. Thus, the MoS_2 and GR cocatalysts had a synergetic effect on the photocatalytic function of the Ag_3PO_4 sub-microcrystals. The following equations describe the major reaction steps involved in this photocatalytic process.

$$Ag_3PO_4 + hv \rightarrow Ag_3PO_4\ (e^- + h^+) \quad (1)$$

$$Ag_3PO_4\ (e^-) + MoS_2\ /GR \rightarrow Ag_3PO_4 + MoS_2\ /GR\ (e^-) \quad (2)$$

$$MoS_2\ /GR\ (e^-) + O_2 \rightarrow MoS_2/\ GR + O_2^- \quad (3)$$

$$Ag_3PO_4\ (h^+) + DCP \rightarrow CO_2 + H_2O + \text{other products} \quad (4)$$

$$Ag_3PO_4\ (h^+) + OH^- \rightarrow Ag_3PO_4 + \cdot OH \quad (5)$$

$$\cdot OH + DCP \rightarrow CO_2 + H_2O + \text{other products} \quad (6)$$

4. Conclusions

We synthesized a layer-structured MoS_2/GR hybrid as an effective cocatalyst for the modification of Ag_3PO_4 sub-microcrystals using a facial two-step hydrothermal method. The Ag_3PO_4-MoS_2/GR composite catalyst exhibited much greater photocatalytic activity than the pure Ag_3PO_4 in organic phenol degradation. Ag_3PO_4-0.02(MoS_2/0.005GR) was the most effective catalyst for the DCP decomposition under simulated solar light and visible light. The optimized photocatalyst was also shown to be highly active in the degradation of nitrophenol and chlorophenol under visible light ($\lambda \geq 420$ nm). The MoS_2/GR nanosheets in the Ag_3PO_4-based photocatalyst functioned as electron collectors for the interfacial electron transfer, which enhanced the separation of the photo-generated electron-hole pairs. In addition, the presence of MoS_2 and GR provided more active adsorption sites and allowed for the activation of dissolved O_2 for organic degradation. The Ag_3PO_4-MoS_2/GR composite proved to be a promising catalyst material for the photocatalytic degradation of toxic environmental pollutants in water.

Acknowledgements

This research was supported by (1) grant HKU714112E from the Research Grants Council (RGC) of the Government of Hong Kong SAR and (2) project 51308230 from the National Natural Science Foundation of China (NSFC). The technical assistance of Mr. Keith C.H. Wong was highly appreciated.

References

1. M. R. Hoffmann, S. T. Martin, W. Y. Choi and D. W. Bahnemann, *Chem Rev*, 1995, **95**, 69-96.

2. A. Fujishima and K. Honda, *Nature*, 1972, **238**, 37-38.
3. A. Kubacka, M. Fernandez-Garcia and G. Colon, *Chem Rev*, 2012, **112**, 1555-1614.
4. Q. J. Xiang, J. G. Yu and M. Jaroniec, *Chem Soc Rev*, 2012, **41**, 782-796.
5. G. Liu, P. Niu and H. M. Cheng, *Chemphyschem*, 2013, **14**, 885-892.
6. Z. G. Yi, J. H. Ye, N. Kikugawa, T. Kako, S. X. Ouyang, H. Stuart-Williams, H. Yang, J. Y. Cao, W. J. Luo, Z. S. Li, Y. Liu and R. L. Withers, *Nat Mater*, 2010, **9**, 559-564.
7. Y. Bi, S. Ouyang, N. Umezawa, J. Cao and J. Ye, *J Am Chem Soc*, 2011, **133**, 6490-6492.
8. X. F. Yang, H. Y. Cui, Y. Li, J. L. Qin, R. X. Zhang and H. Tang, *Acs Catal*, 2013, **3**, 363-369.
9. L. Liu, J. C. Liu and D. D. Sun, *Catal Sci Technol*, 2012, **2**, 2525-2532.
10. H. Q. Cao, B. J. Li, J. X. Zhang, F. Lian, X. H. Kong and M. Z. Qu, *J Mater Chem*, 2012, **22**, 9759-9766.
11. T. Lv, L. K. Pan, X. J. Liu, T. Lu, G. Zhu, Z. Sun and C. Q. Sun, *Catal Sci Technol*, 2012, **2**, 754-758.
12. K. S. Novoselov, A. K. Geim, S. V. Morozov, D. Jiang, Y. Zhang, S. V. Dubonos, I. V. Grigorieva and A. A. Firsov, *Science*, 2004, **306**, 666-669.
13. Z. Chen, S. Q. Liu, M. Q. Yang and Y. J. Xu, *Acs Applied Materials & Interfaces*, 2013, **5**, 4309-4319.
14. W. C. Peng and X. Y. Li, *Nano Res*, 2013, **6**, 286-292.
15. Q. J. Xiang, J. G. Yu and M. Jaroniec, *J Am Chem Soc*, 2012, **134**, 6575-6578.
16. T. F. Jaramillo, K. P. Jorgensen, J. Bonde, J. H. Nielsen, S. Horch and I. Chorkendorff, *Science*, 2007, **317**, 100-102.
17. T. T. Jia, A. Kolpin, C. S. Ma, R. C. T. Chan, W. M. Kwok and S. C. E. Tsang, *Chem Commun*, 2014, **50**, 1185-1188.
18. L. Ge, C. Han and J. Liu, *Applied Catalysis B: Environmental*, 2011, **108**, 100-107.
19. L. Ge, C. C. Han, X. L. Xiao and L. L. Guo, *Int J Hydrogen Energ*, 2013, **38**, 6960-6969.
20. Q. S. Gao, C. Giordano and M. Antonietti, *Angew Chem Int Edit*, 2012, **51**, 11740-11744.
21. X. Zong, H. J. Yan, G. P. Wu, G. J. Ma, F. Y. Wen, L. Wang and C. Li, *J Am Chem Soc*, 2008, **130**, 7176-7177.

22. I. Tacchini, E. Terrado, A. Anson and M. T. Martinez, *Micro Nano Lett*, 2011, **6**, 932-936.
23. X. Zong, G. P. Wu, H. J. Yan, G. J. Ma, J. Y. Shi, F. Y. Wen, L. Wang and C. Li, *J Phys Chem C*, 2010, **114**, 1963-1968.
24. K. H. Hu, Z. Liu, F. Huang, X. G. Hu and C. L. Han, *Chem Eng J*, 2010, **162**, 836-843.
25. D. Cropek, P. A. Kemme, O. V. Makarova, L. X. Chen and T. Rajh, *J Phys Chem C*, 2008, **112**, 8311-8318.
26. M. S. Yalfani, A. Georgi, S. Contreras, F. Medina and F. D. Kopinke, *Appl Catal B-Environ*, 2011, **104**, 161-168.
27. S. Gazi and R. Ananthakrishnan, *Appl Catal B-Environ*, 2011, **105**, 317-325.
28. D. W. Chen and A. K. Ray, *Water Res*, 1998, **32**, 3223-3234.
29. M. Czaplicka, *J Hazard Mater*, 2006, **134**, 45-59.
30. W. S. Hummers Jr and R. E. Offeman, *J Am Chem Soc*, 1958, **80**, 1339-1339.
31. Y. G. Li, H. L. Wang, L. M. Xie, Y. Y. Liang, G. S. Hong and H. J. Dai, *J Am Chem Soc*, 2011, **133**, 7296-7299.
32. O. Akhavan, M. Abdolahad, A. Esfandiar and M. Mohatashamifar, *J Phys Chem C*, 2010, **114**, 12955-12959.
33. T. N. Zhou, F. Chen, K. Liu, H. Deng, Q. Zhang, J. W. Feng and Q. A. Fu, *Nanotechnology*, 2011, **22**, 045704-045709.
34. Z. H. Zhao, J. Tian, D. Z. Wang, X. L. Kang, Y. H. Sang, H. Liu, J. Y. Wang, S. W. Chen, R. I. Boughton and H. D. Jiang, *J Mater Chem*, 2012, **22**, 23395-23403.
35. J. Tian, Y. Sang, Z. Zhao, W. Zhou, D. Wang, X. Kang, H. Liu, J. Wang, S. Chen, H. Cai and H. Huang, *Small*, 2013, **9**, 3864-3872.
36. H. Y. Hu, Z. B. Jiao, H. C. Yu, G. X. Lu, J. H. Ye and Y. P. Bi, *Journal of Materials Chemistry A*, 2013, **1**, 2387-2390.
37. Y. H. Zhang, Z. R. Tang, X. Z. Fu and Y. J. Xu, *Acs Nano*, 2010, **4**, 7303-7314.
38. Q. Li, B. D. Guo, J. G. Yu, J. R. Ran, B. H. Zhang, H. J. Yan and J. R. Gong, *J Am Chem Soc*, 2011, **133**, 10878-10884.
39. N. S. Kumar and K. Min, *Chem Eng J*, 2011, **168**, 562-571.

40. Q. Xiang, J. Yu and M. Jaroniec, *Nanoscale*, 2011, **3**, 3670-3678.

41. J. C. Liu, H. W. Bai, Y. J. Wang, Z. Y. Liu, X. W. Zhang and D. D. Sun, *Adv Funct Mater*, 2010, **20**, 4175-4181.

Electronic Supplementary Information

Synergetic Effect of MoS_2 and Graphene on Ag_3PO_4 for its Ultra-Enhanced Photocatalytic Activity in Phenols Degradation under Visible Light

Wen-chao Peng [1], Xi Wang [1,2] and Xiao-yan Li[1]*

[1] Environmental Engineering Research Centre, Department of Civil Engineering, The University of Hong Kong, Pokfulam Road, Hong Kong

[2] School of Chemistry and Environment, South China Normal University, Guangzhou, Guangdong, China

(*Corresponding author: phone: 852 2859-2659; fax: 852 2859-5337; e-mail: xlia@hkucc.hku.hk)

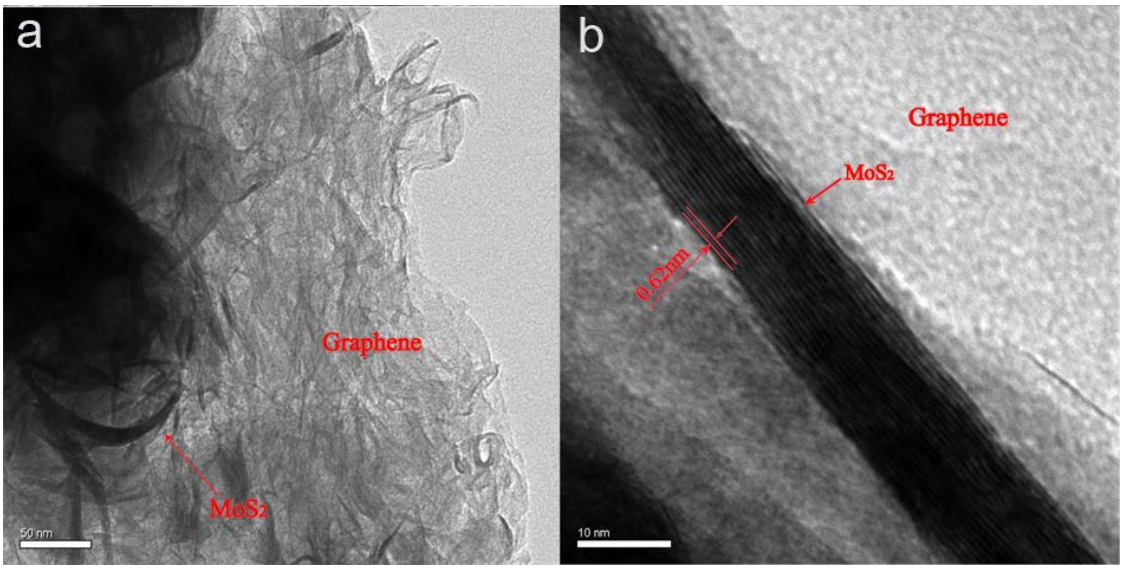

Fig. S1. Morphology of the MoS_2/GR hybrid: (a) TEM images in large magnifications of the layered MoS_2/GR hybrid; (b) high-resolution TEM image of the hybrid showing the close contact between the MoS_2 and GR.

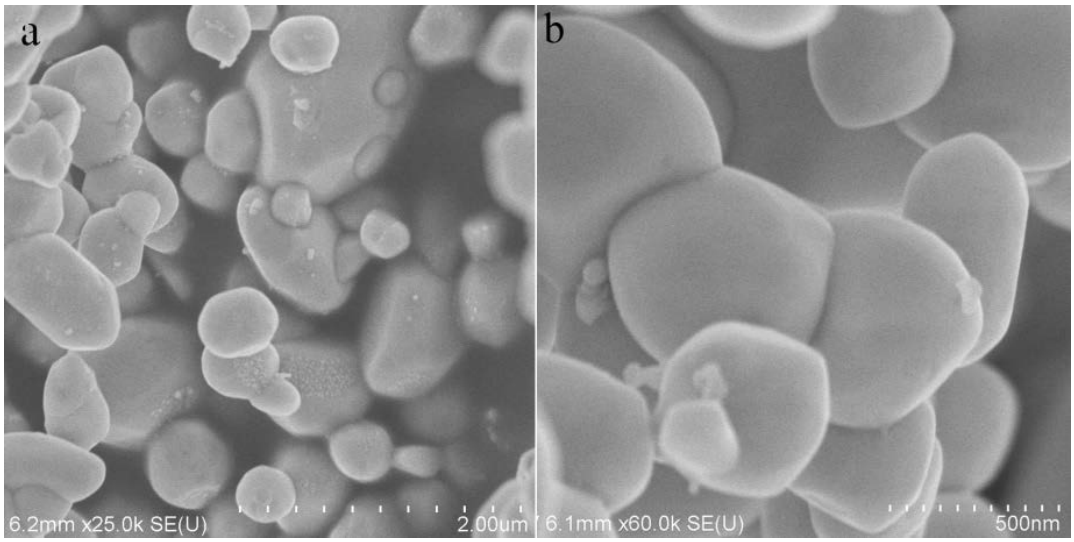

Fig. S2. (a) and (b) SEM images of the pure Ag_3PO_4 crystals at different magnifications

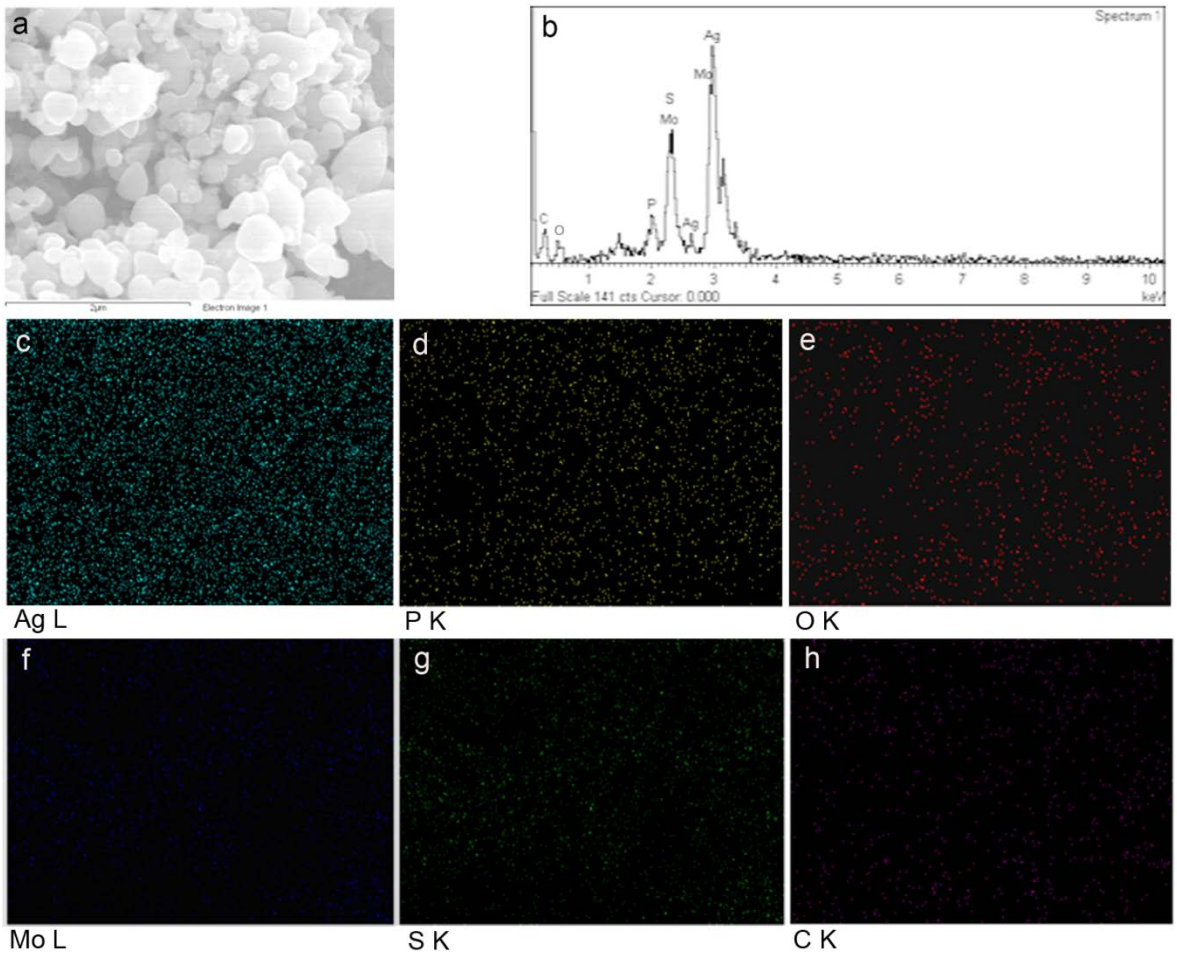

Fig. S3. Elemental analysis for Ag_3PO_4-MoS_2/GR composite: (a) SEM image of the mapping area; (b) EDX spectra of the Ag_3PO_4-MoS_2/GR composite; (c)-(h) EDX elementary mapping of Ag, P, O, Mo, S and C in Ag_3PO_4-MoS_2/GR composite.

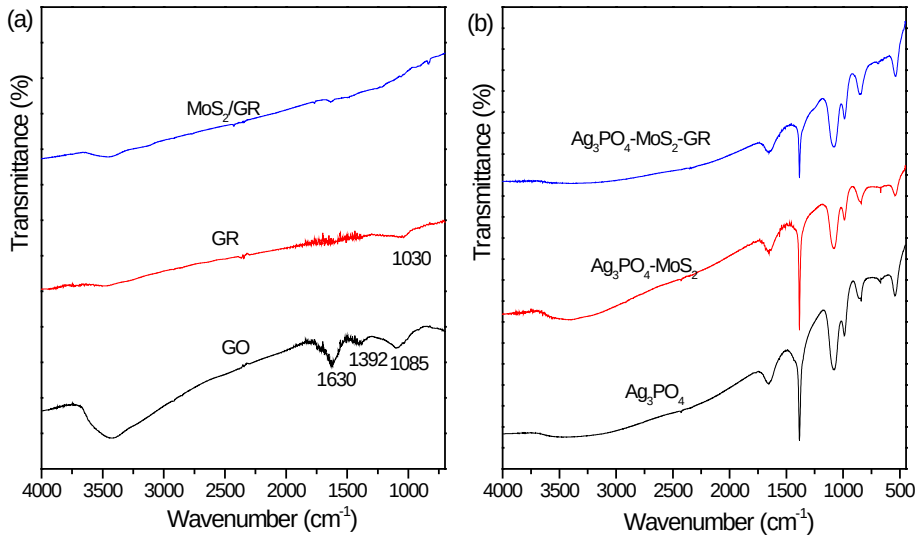

Fig. S4. (a) FT-IR spectra of the GO, GR and MoS_2/GR hybrid (note: most of the functional groups were removed for the GO, indicating a successful reduction from GO to GR); (b) FT-IR spectra for the pure Ag_3PO_4 and composites (note: there were no new chemical bonds formed during the composite preparation process).

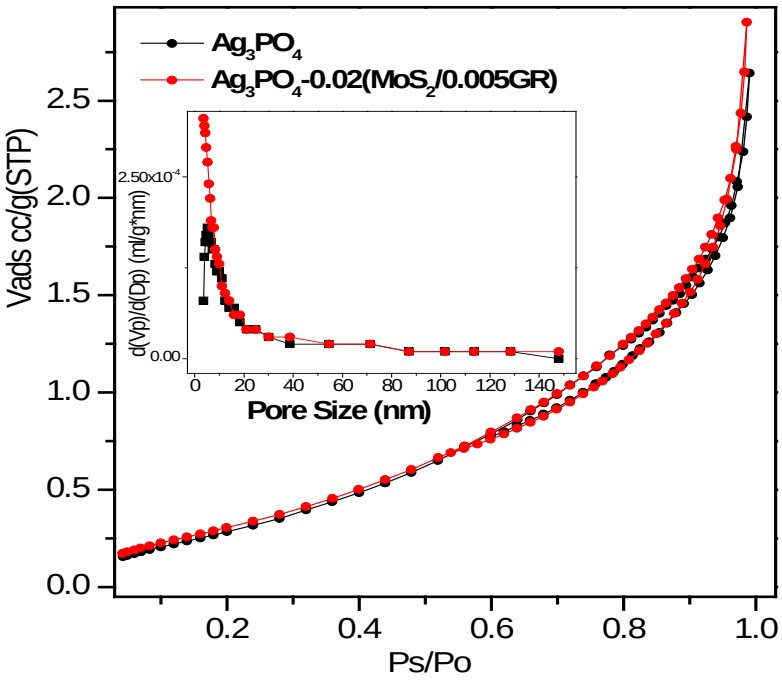

Fig. S5. N_2 adsorption tests for the pure Ag_3PO_4 and Ag_3PO_4-MoS_2/GR composite. A slight increase in adsorption capability was found after the MoS_2/GR addition. However, the pore structure was nearly the same. The surface areas of Ag_3PO_4 and Ag_3PO_4-0.02(MoS_2/0.005GR) composite were 1.1 and 1.2 m^2/g, respectively, and the total pore volumes (Ps/Po = 0.9814, Adsorption) were 0.0035 and 0.0040 ml/g for these two respective photocatalyst materials.

Photoelectric Conversions

The photoelectric conversion property was investigated on the photocatalyst materials using a three-electrode cell connected to a computer-controlled potentiostat (Princeton VersaSTAT 4). To make a working electrode for a catalyst material, 50 mg of the catalyst powder, 2.5 mg carbon black and 5 mg polyvinylidene difluoride (PVDF) were first mixed into 0.5 mL N,N-Dimethylmethanamide (DMF). The mixture was ultrasonically dispersed for 15 min, and 0.1 mL of the solution was then dropped on a tin-doped indium oxide (ITO) glass slide (1.5×1 cm). After evaporation of the DMF, the catalyst was left that attached firmly onto the surface of the ITO glass. For the photocurrent measurement on the working electrode, a Pt film (2×1 cm) was used as the counter-electrode, an Ag/AgCl electrode was used as the counter-electrode, and all three electrodes were immersed in 0.01 M sodium sulfate as the electrolyte. The light source had a 300W Xe lamp with a cutoff filter of 420 nm inserted for the visible-light irradiation. The photocurrent density was detected by the potentiostat, and the current-time (i-t) curves were obtained without bias.

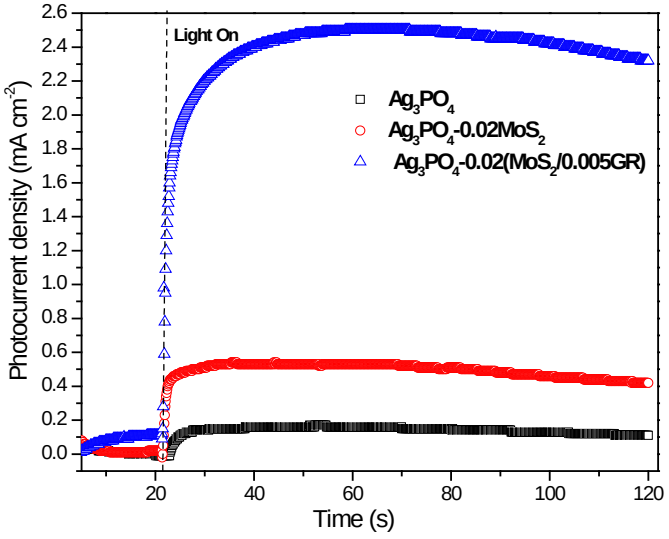

Fig. S6. The transient photocurrents of the Ag_3PO_4, Ag_3PO_4-MoS_2 and Ag_3PO_4-MoS_2/GR electrodes in 0.01 M Na_2SO_4 aqueous solution under visible light (λ>420 nm) without bias versus Ag/AgCl as the reference electrode.

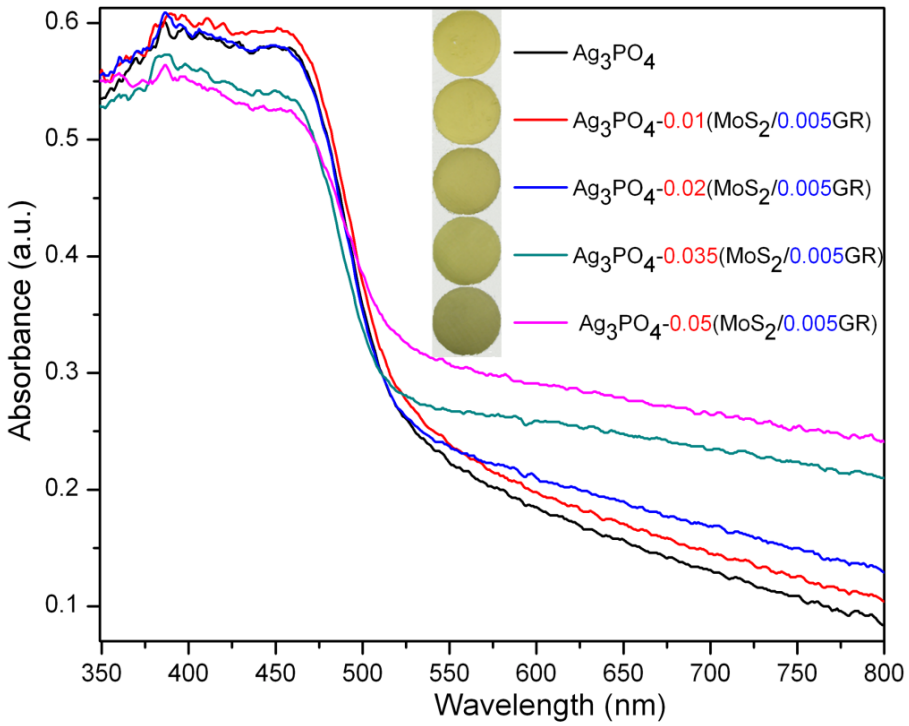

Fig. S7. UV-vis diffusive reflectance spectra of the Ag_3PO_4 and Ag_3PO_4-MoS_2/GR composites. The composites exhibited a stronger absorption capability in the visible light region as the MoS_2/GR co-catalyst content increased. This was in agreement with the color change of the composites from light green to dark green, as indicated by the inset images.

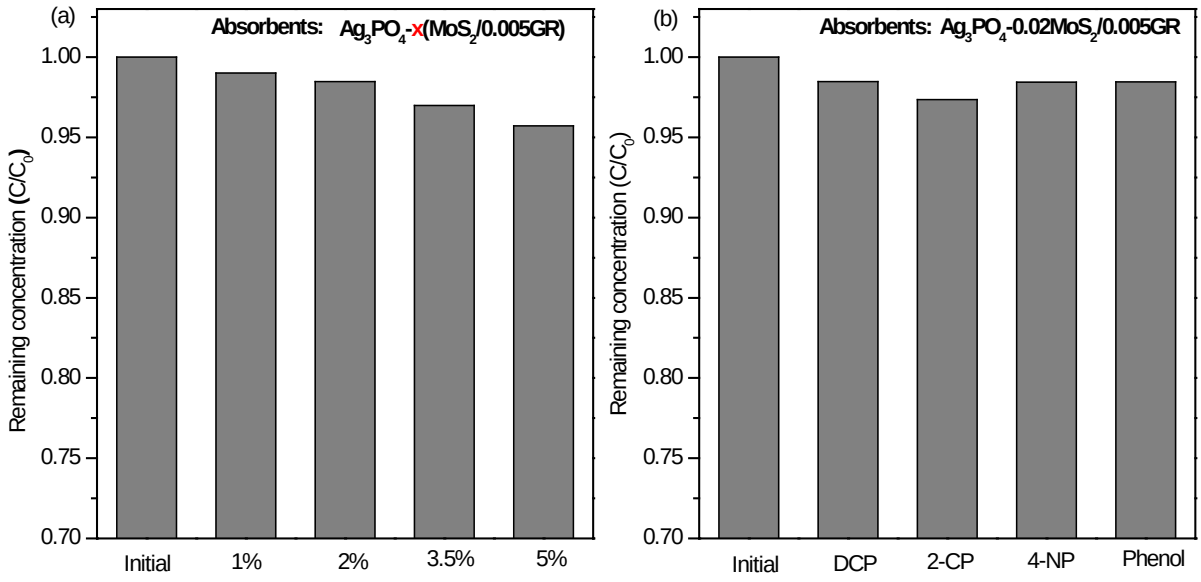

Fig. S8. (a) Change in DCP concentration after adsorption in the dark by the Ag_3PO_4-based catalysts with different MoS_2/0.005GR percentages; (b) Change in concentration for different phenols after adsorption in the dark by Ag_3PO_4-0.02(MoS_2/0.005GR).

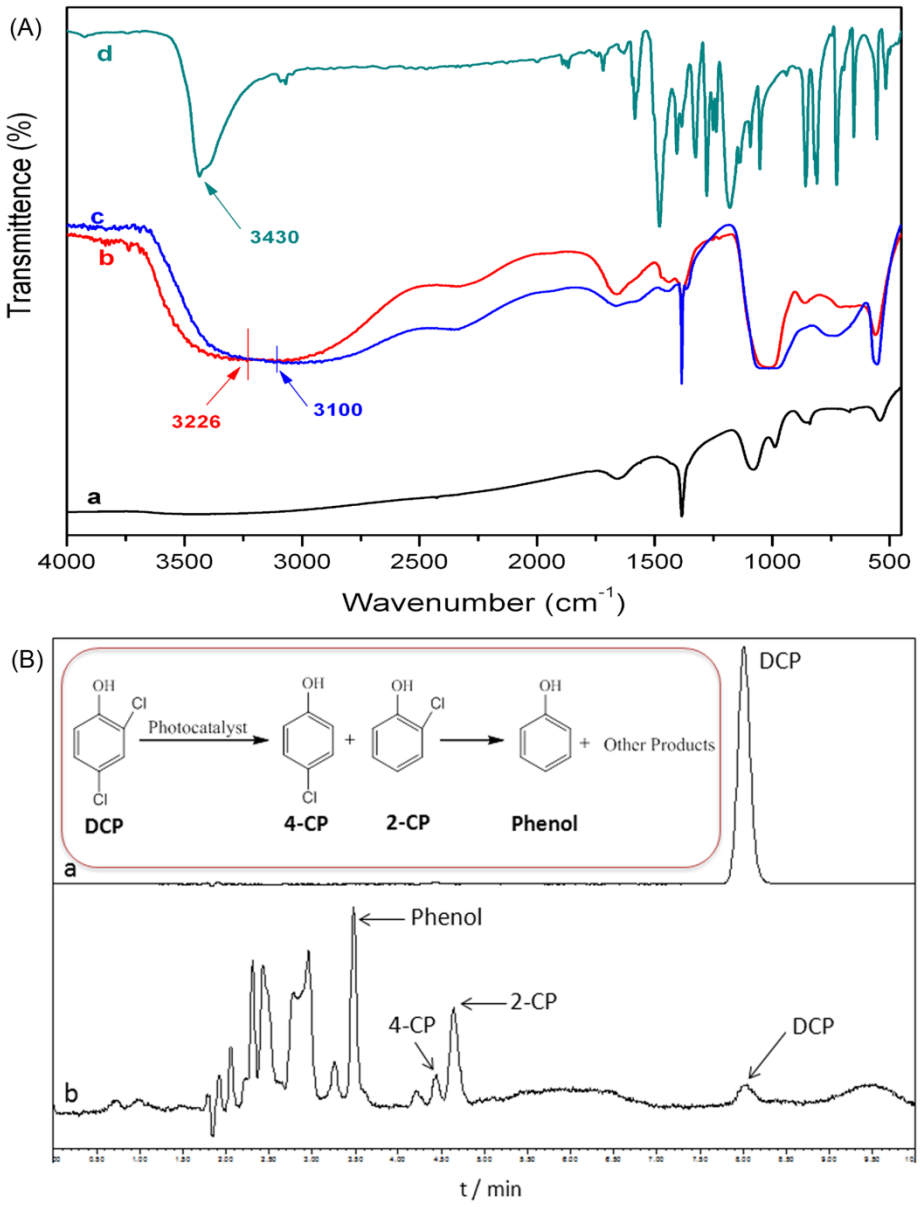

Fig. S9 (A) FT-IR spectra of (a) the Ag_3PO_4-0.02(MoS_2/0.005GR) photocatalyst suspension, (b) Ag_3PO_4-0.02(MoS_2/0.005GR) photocatalyst mixing in the DCP solution in the dark for 4 h, (c) Ag_3PO_4-0.02(MoS_2/0.005GR) photocatalyst mixing in the DCP solution in the dark for 4 h and then under visible light for 1 h, and (d) pure DCP solution; (B) HPLC spectra of the DCP solution (a) before degradation and (b) after the photo-degradation; inset of Fig. B is the proposed mechanism of photocatalytic DCP degradation.

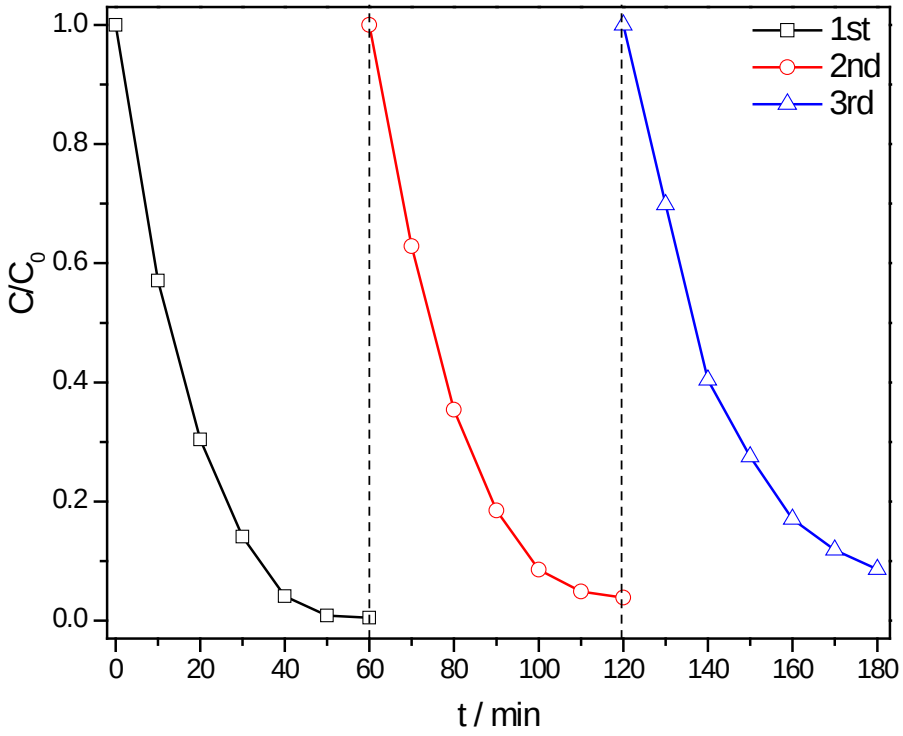

Fig. S10. The stability and reactivity of the recycled Ag_3PO_4-0.02(MoS_2/0.005GR) catalyst as demonstrated by the repeated tests of photocatalytic DCP degradation.

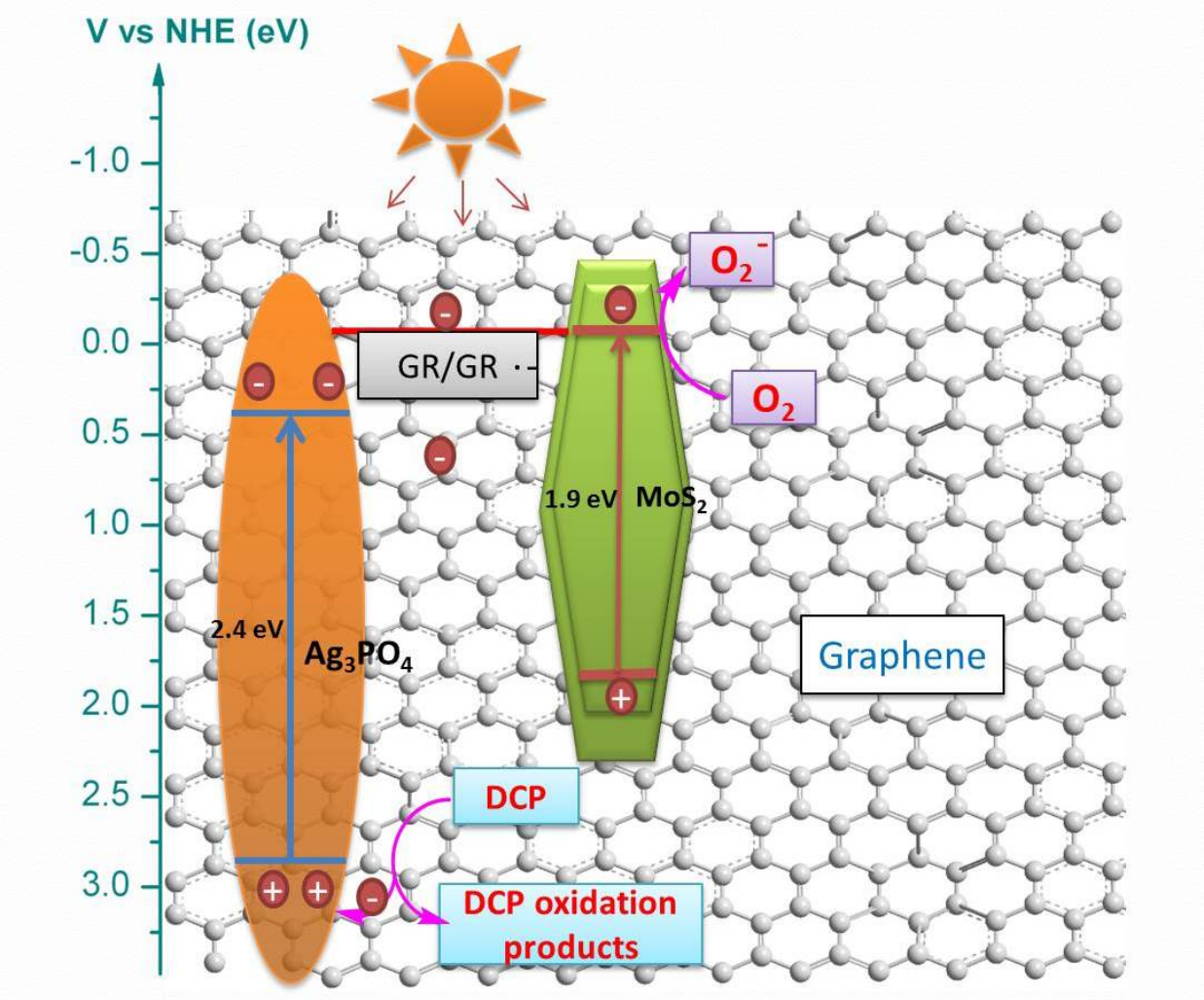

Fig. S11. Schematic illustration of the energy diagram and electron transfer scheme for the photocatalytic DCP degradation by the Ag_3PO_4-MoS_2/GR composite.